ICES Journal of Marine Science, 62: 634–644 (2005)
doi:10.1016/j.icesjms.2005.02.007

Survival of sardine larvae off the Atlantic Portuguese coast: a preliminary numerical study

Aires J. P. Santos, João Nogueira, and Helder Martins

Santos, A. J. P., Nogueira, J., and Martins, H. 2005. Survival of sardine larvae off the Atlantic Portuguese coast: a preliminary numerical study. – ICES Journal of Marine Science, 62: 634–644.

A bio-physical model of sardine larvae off the Atlantic Portuguese coast, incorporating a three-dimensional circulation model, was used to estimate changing biomass during winter upwelling and downwelling events. The growth rate of larvae was modelled as a function of age, temperature, and prey concentration and the mortality rate as a function of age and temperature. Numerical results indicate that upwelling events during the spawning season may have a negative impact on larval survival. Total larval biomass seems to be mainly controlled by larval prey relative to temperature. This preliminary study does not account for the dynamics of the food chain and therefore the intense biological activity associated with an upwelling event, as well as the influence of river plumes in retention mechanisms.

Keywords: biomass, downwelling, growth, larvae, mortality, upwelling.

Received 11 June 2003; accepted 14 February 2005.

A. J. P. Santos and H. Martins: Department of Mechanical Engineering, Instituto Superior Técnico, Av. Rovisco Pais, Lisboa, Portugal. J. Nogueira: Department of Natural and Biological Science, Universidade Lusófona de Humanidades e Tecnologias, Campo Grande, Lisboa, Portugal. Correspondence to A. J. P. Santos: tel: +351 21 841 79 86; fax: +351 21 841 73 98; e-mail: aires@popsrv.ist.utl.pt.

Introduction

Fish pass through different stages and successively display a state of being passive particles (eggs and yolk-sac larvae), zooplankton (larvae and early juveniles), and finally nekton (older juveniles and adults). Knowledge of the life cycle and interannual stock variations are important tools for fishery management. Fishery productivity is related to the underlying stock-recruitment relationship, but this function is non-linear and the factors that regulate it are not directly correlated (Lett and Kohler, 1976; Mohn, 1991; Myers, 1991). Fish biomass varies not only from year to year but also over long periods. Physical processes play a significant role in determining larval survival. Larval transport away from favourable nursery areas and mass starvation of larvae at the time that feeding must be initiated are potential causes of extreme variations in year-class strength.

Over the last decades significant changes in upwelling patterns off the Portuguese west coast have been observed (Dickson *et al.*, 1988; Santos *et al.*, 2001; Borges *et al.*, 2003). Santos *et al.* (2001) reported that decreasing trends in sardine and horse mackerel recruitment off the Portuguese coast in the 1980s and 1990s were related to an increasing trend in SST upwelling indices during winter (January–March), especially between 1992 and 1995. Bakun (1996) suggested that upwelling intensity was linked to large-scale climatic effects. Borges *et al.* (2003) found a highly significant correlation between the NAO index and wind conditions off Portugal during winter. During the early 1990s the NAO increased to positive values higher than previously recorded, and this was reflected in more intense winter upwelling conditions off the west coast of Portugal, leading to the lowest recruitment (1991–1996) observed since 1978 (Santos *et al.*, 2001).

Various modelling studies have shown the important role of circulation in recruitment success. Such numerical simulations are the best way to tackle the prediction of larval dispersal because they can account for realistic coastal geometry and bottom topography, as well as temporal and spatial variations in advection and turbulence fields. A three-dimensional hydrodynamic circulation model (Backhaus, 1985) based on the HAMburg Shelf Ocean Model (HAMSOM), coupled to a random walk transport model for the diffusion process and a vertical migration model for larvae, was used to study the dispersion of North Sea herring larvae (Bartsch *et al.*, 1989) and blue whiting larvae in the eastern North Atlantic (Bartsch and Coombs, 1997). Heath and Gallego (1998) considered an individual-based modelling approach to investigate the spatial and temporal patterns in the recruitment processes of North Sea

1054-3139/$30.00

haddock. The HAMSOM circulation model provided a three-dimensional flow that served as input to the transport model, and the biological component was a combination of a model of egg production by the adult stock and a model of temperature-dependent larval growth and mortality.

The present study was carried out as part of the project SURVIVAL (*Assessing the Impact of Hydrodynamical Forcing on the Survival of Small Pelagic Fish Early Stages of Western Iberia*). SURVIVAL was intended to be a contribution, at national level, for the International Global Ocean Ecosystem Dynamics (GLOBEC) Programme on Small Pelagic Fish and Climate Change. The objectives were: (i) studying the hydrodynamic impact on egg–larvae dispersal and survival upon different stratification and atmospheric forcings; (ii) studying the circulation structure and associated egg and larvae transport during a winter upwelling event; (iii) developing the basis of an early life transport and survival model. In this study a three-dimensional hydrodynamic circulation model (MOHID2000) was applied to the Atlantic coasts of the Iberian Peninsula, for the main spawning season (winter) of sardine off the northern Portuguese coast. A formal comparison of model results with field observations was beyond the scope of this study. The circulation model was run using climatological density fields as well as both constant northerly windstress and realistic six-hourly windstress fields from the European Centre for Medium-Range Weather Forecasting (ECMWF) for 1994, one of the years with the highest winter upwelling indices (Santos *et al.*, 2001). The three-dimensional flow served as input to the transport model. Larval growth rate was modelled as a function of age, temperature, and prey concentration, and larval mortality rate was modelled as a function of age and temperature.

Material and methods

Circulation model

The hydrodynamic model MOHID2000 used in this work (Santos, 1995; Martins *et al.*, 1998; Martins *et al.*, 2000) solves the equations of a three-dimensional flow for incompressible fluids and an equation of state relating density to salinity and temperature (Leendertsee and Liu, 1978). Hydrostatic equilibrium and the Boussinesq approximation are assumed. The model uses a semi-implicit ADI algorithm with two time levels per iteration. For this study the biharmonic operator proved to be more appropriate for horizontal diffusion of heat, salt, and momentum for the spatial scales involved. Bottom stress was parameterized using a quadratic law. Vertical eddy viscosity/diffusivity was determined with a turbulence closure model selected from those available in the General Ocean Turbulence Model (Burchard *et al.*, 1999).

In this study, a simplified version of the model proposed by Gaspar *et al.* (1990) was used, because it gives reasonable results without excessively increasing CPU resources. Horizontal grid spacing is 8 km in both directions. Bottom topography was derived from ETOPO5 by means of an interpolation for the model grid followed by smoothing with a five-point Laplacian filter. The bottom depth is then determined, using shaved cells (Adcroft *et al.*, 1997). The model allows several options for the vertical discretization: Cartesian coordinates, sigma coordinates or a generic vertical coordinate. In this study a Cartesian coordinate was chosen with 15 vertical layers. Thicknesses from top to bottom are 2, 2, 2, 2, 2, 4, 6, 10, 20, 50, 100, 200, 600, 2000, 2000 m. The biharmonic momentum diffusion coefficient is equal to $2 \times 10^9\ m^4\ s^{-1}$, the same value applied by Batteen *et al.* (2000), with a similar horizontal resolution and horizontal diffusivity for salinity and temperature equal to $350\ m^2\ s^{-1}$. Normal and tangential velocities are set to zero at the sidewalls.

The open boundary conditions for sea surface height, barotropic velocity, baroclinic velocity, temperature, and salinity used were very similar to the FOA scheme conceived by Oey and Chen (1992) and Palma and Matano (2000). It sets the barotropic transport at the open boundary in accordance with the density field, at the same time as allowing waves generated inside the domain to radiate out. The barotropic velocities at the open boundary are deduced from steady seasonal transports. Additionally, we used the radiation condition proposed by Flather (1976) for the normal component of barotropic velocity. Sommerfeld's one-dimensional radiation condition was applied for the normal baroclinic velocities at the boundary. Our boundary condition for scalars was the same as that proposed by Oey and Chen (1992). Along with this set of boundary conditions, some of the prognostic variables are relaxed to climatology by applying a relaxing term in the prognostic equations near the open boundaries.

In order to implement the set of boundary conditions described above we need to compute external values for the prognostic variables. For the scalars (temperature and salinity), the external data are the same as used for model initialization at the boundaries. The data are interpolated in time for the model time-step, allowing the boundary condition to be variable in time. To determine the barotropic velocities, a level of no motion at 2500 m is assumed, according to Paillet and Mercier (1997) and Arhan *et al.* (1994). Knowing the depth mean currents and the density field, we calculated the external baroclinic velocities normal to the boundary by assuming the thermal wind relation. Finally, since barotropic transport is known, sea surface height is calculated from the vertically integrated geostrophic relation. The model was initialized from a state of no motion with mean winter climatological temperature and salinity fields. The climatological temperature and salinity fields are extracted from Levitus *et al.* (1994) and interpolated to the model grid before smoothing with a simple cubic spline algorithm. Besides climatological density, the model was forced with data from the European Centre for Medium-Range Weather Forecasts (ECMWF)

(Trenberth *et al.*, 1990) using daily momentum fluxes from the ECMWF large-scale forecast model for the year 1994. Results were compared with the numerical solution obtained by forcing the computational domain with a northerly constant windstress (downwelling regime) of 0.1 Pa. The spatial resolution of the ECMWF fluxes is 1° by 1°. The data were interpolated spatially for the model grid and temporally for the model time-step.

Transport model

A Lagrangian model was coupled with the circulation model to describe the movement of larvae. The tracers' trajectories were determined solely by advective dispersal, because Heath and Gallego (1997) showed that diffusion has only a second-order effect on the results in terms of modelled growth rates of larvae.

Larval model

The transport equation for total larval biomass is:

$$\frac{\partial B}{\partial t}+\frac{\partial(uB)}{\partial x}+\frac{\partial(vB)}{\partial y}+\frac{\partial((w+w')B)}{\partial z}=k_1k_2(GB)-k_3(ZB) \quad (1)$$

where B denotes biomass, u, v, and w are the components of the velocity vector, w′ is the vertical velocity associated with the vertical migration of larvae (in this study we considered $w' = 0$), G (d^{-1}) is the weight-specific growth coefficient, Z (d^{-1}) is the instantaneous daily mortality coefficient, k_1 is a correction coefficient taking into account food availability, and k_2, k_3 are correction coefficients for the effect of water temperature (T) on growth and mortality.

The larval model computes the sink and source terms of Equation (1); the left hand side of this equation was calculated using the circulation model. Eggs and larvae are the life stages that typically exhibit the highest and most variable mortality. Cohort biomass declines while $Z/G > 1$, until a transition size at $Z/G = 1$ is achieved, after which biomass increases when $Z/G < 1$ (Cowan *et al.*, 1999). Houde (1989) and Pepin (1991) reviewed the literature pointing out the correlation between G and Z and their strong dependence upon temperature and body size. Houde (1996) also concluded that the Z/G ratio links the population dynamics and bioenergetics processes in early life, and is sensitive to consumption rates (food abundance) and assimilation rates (food quality) that larvae experience. For northern anchovy from the eastern Pacific, Houde (1997) proposed power equations for Z and Z/G:

$$Z=1.073W^{-0.353} \quad (2)$$

$$Z/G=7.983W^{-0.292} \quad (3)$$

where W (μg) is the individual body weight. These equations were applied to our study of sardine larvae on the Portuguese coast, and yielded a growth coefficient equal to:

$$G=0.1344W^{-0.061} \quad (4)$$

Therefore it is possible to compute time-dependent growth and mortality coefficients, knowing larval length as a function of age and where a length–weight relationship has been determined. For the Pacific sardine *Sardinops sagax*, Lo *et al.* (1995) report larval length as a function of age (Table 1); stages 3 and 4 are relevant to our study. For the length–weight relationship, we applied the following equation (Ribeiro, 1991):

$$W=\exp(-2.95+3.78\ln L) \quad (5)$$

We used the temperature-dependent relationships for G and Z from Houde and Zastrow (1993):

$$G=0.0511+0.0052T \quad (6)$$

$$Z=0.0149+0.0129T \quad (7)$$

from which it is possible to derive equations for the correction coefficients k_2, k_3. Differentiating Equation (6) with respect to temperature and considering a modal value for temperatures of 15 °C, the values from Table 1, after Lo *et al.* (1995), yield:

$$\frac{dG}{dT}=0.0052 \Rightarrow G=G_{15}+0.0052\Delta T=k_2G_{15}$$

where $\Delta T = T - 15$. This yields:

$$k_2=1+\frac{0.0052}{G_{15}}\Delta T \quad (8)$$

Table 1. Stage duration and length for Pacific sardine *Sardinops sagax* (after Lo *et al.*, 1995).

Stage	Name	Duration (days)	Length (mm)
1	Egg	2.5	
2	Yolk sac	3.1	−4
3	Early larvae	11.0	5–10
4	Late larvae	35.0	11–35
5	Early juvenile	25.0	36–60
6	Juvenile I	50.0	61–85
7	Juvenile II	110.0	86–110
8	Juvenile III	146.0	111–135
9	Juvenile IV	170.0	136–160
10	Pre-recruitment	175.0	161–185
11	Early adult	381.0	186–210
12	Adult	663.0	211–235
13	Late adult	2773.0	236–250

and

$$k_3 = 1 + \frac{0.0129}{Z_{15}}\Delta T \qquad (9)$$

Equations (8) and (9) assume that, for a temperature of 15°C, the coefficients are $k_2 = k_3 = 1$. The dependence of growth on larval prey can be parameterized according to a Michaelis–Menten equation:

$$k_1 = \frac{1}{k_1'}\left(\frac{F}{a+F}\right) \quad \text{with } k_1' = \frac{F_{max}}{a+F_{max}} \qquad (10)$$

where $a = 0.1\ mg\,m^{-3}$ is the half-saturation constant. In this study, larval prey concentration and position were held constant throughout the simulation period. The initial values were bounded between $0.5\ mg\,m^{-3}$ near the surface and $0.005\ mg\,m^{-3}$ near 200-m depth (or 100 m), in the region of the continental shelf (Moita, 2001). For the open ocean a constant concentration of $0.005\ mg\,m^{-3}$ was set from the sea surface to a depth of 200 m (or 100 m). In either case (deep or coastal) the concentration was assumed to be zero below this depth. From Equation (10), $k_1 = 1$ when $F = F_{max} = 0.5\ mg\,m^{-3}$ and $k_1 = 0$ when $F = 0$.

For the initial total larval biomass a value of 7200×10^3 kg was assumed, distributed from the surface to a depth of 100 m in the Aveiro region. According to Ré (1986), the spawning period for *Sardina pilchardus* off the Portuguese coast extends throughout the whole year but maximum biomass is in winter (December–January). Water temperature in winter is coincident with the optimal water temperature range for maximum spawning (13.8–15.4°C). Larval growth rate values for the Pacific sardine *Sardinops sagax* ($0.65\ mm\,d^{-1}$; Table 1) are similar to those obtained for *Sardina pilchardus* ($0.59\ mm\,d^{-1}$; Alemany and Álvarez, 1994).

Simulations

The effect of four variables on the growth and survival of sardine larvae were tested in these simulations: (i) windfield; (ii) water depth where larval prey is concentrated; (iii) water temperature, and (iv) concentration of larval prey. For the windfield, we compared an "anomalous" year, with strong winter upwelling events, to a "normal" year, when winter downwelling prevails. In order to emphasize the differences between these two wind patterns, a comparison was made between a real wind simulation and a constant northerly wind simulation with a meridional windstress equal to 0.1 Pa. This windstress corresponds roughly to a northerly windspeed of $7\ m\,s^{-1}$, which is consistent with the mean winter value observed for 1931–1960 at Cape Carvoeiro (Ferreira, 1970) near Aveiro, where the tracers of this numerical study were released. For the real wind simulation, data were obtained from the ECMWF for 1994, considered one of the "anomalous" years. The simulation began at the end of February and lasted 60 days, which corresponds to the initial spin-up of the model plus the larval period (45 days).

At the latitude of our study the winter surface mixed layer usually lies between 100 m and 200 m. As we have no information on the vertical distribution of larval sardine prey, numerical simulations were therefore performed with a constant larval prey layer thickness throughout the simulation period and equal to 100 m or 200 m. In both cases, tracers representing sardine larvae were released in the top 100 m, where spawning occurs (Ré, 1986). To determine the relative effects of temperature and food availability on larval growth and mortality rates, we successively set the effects of each variable (k_1 for prey; k_2 and k_3 for temperature) to a value of 1, independent of spatial or temporal variations in environmental conditions. Relative changes of biomass, $e_{ij} = (B_i - B_j)/B_j$, were computed (Table 2) in order to compare the simulations.

Results

The meridional and zonal windstress components near Cape Finisterra, for a 45-day period starting on 27 February 1994 (Figure 1), show that this was a period of intense winter upwelling, and only around day 30 did northerly winds persist, for little more than 3 days, near Cape Finisterra. Figure 2a shows the initial position of larvae at Aveiro. After 34 days of real wind, tracers are distributed along the coast reaching the most northern position shortly after the downwelling event represented in Figures 1a and 3a. Many particles have been advected south along the Portuguese coast and into offshore regions (Figure 2b). By contrast, after 34 days of constant northerly winds with a windstress equal to 0.1 Pa, tracers are more distributed further north. The constant northerly wind simulation indicates a larval drift from the northern Portuguese coast to the Galician coast and a strong northward current

Table 2. Relative changes of total larval biomass at the end of the simulation (e_{ij}). The indices i and j refer to the number of the curves in Figure 5.

Figures	Simulations	e_{ij} (%)
Figure 5a	North100-Real100	$e_{12} = 5.7$
	North200-Real200	$e_{34} = 30.6$
	Real200-Real100	$e_{42} = 8.5$
	North200-North100	$e_{31} = 33.4$
Figure 5b	Prey-Real100	$e_{31} = 60.0$
	Prey-Real200	$e_{32} = 46.9$
	Temp100-Real100	$e_{41} = -14.2$
	Temp200-Real200	$e_{52} = -13.6$
Figure 5c	Prey-North100	$e_{31} = 52.1$
	Prey-North200	$e_{32} = 8.6$
	Temp100-North100	$e_{41} = -6.4$
	Temp200-North200	$e_{52} = -8.4$

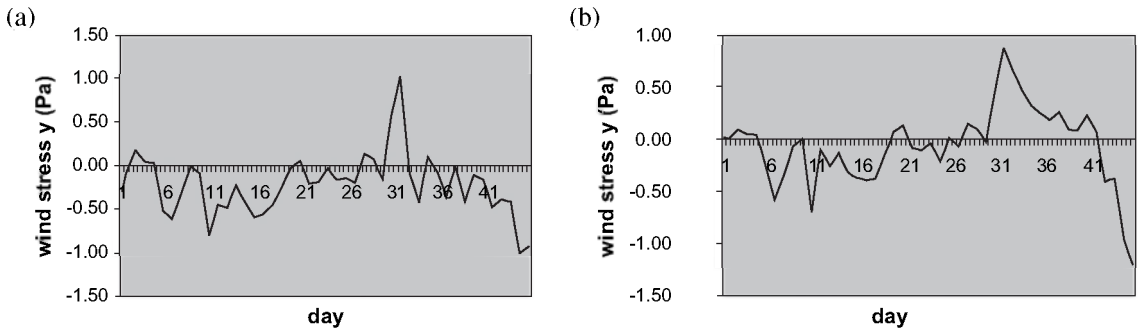

Figure 1. Meridional (a) and zonal (b) windstress at 42.5°N, 9.4°W.

(Figures 2c and 3c). At day 44 in the real wind simulation, a typical upwelling event with cold water near the coast and offshore transport is present (Figure 3b), showing little memory of the short-term downwelling wind conditions. Vigo Bank is also visible in the region of the anticyclonic gyre. The dispersion of the tracers for different wind regimes shows the percentage of tracers that went offshore, crossing the 1000-m isobath (Figure 4). For the northerly

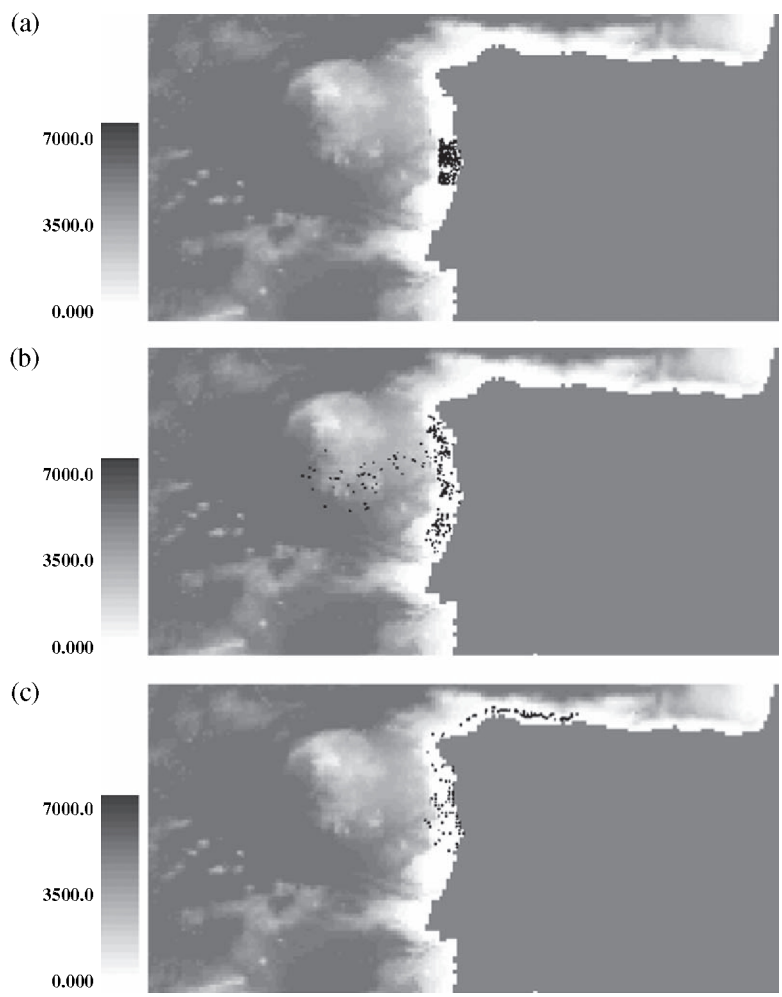

Figure 2. (a) Initial position of the tracers; (b) position of the tracers after 34 days of real wind; (c) position of the tracers after 34 days of northerly wind. The grey scale bar indicates depth (m).

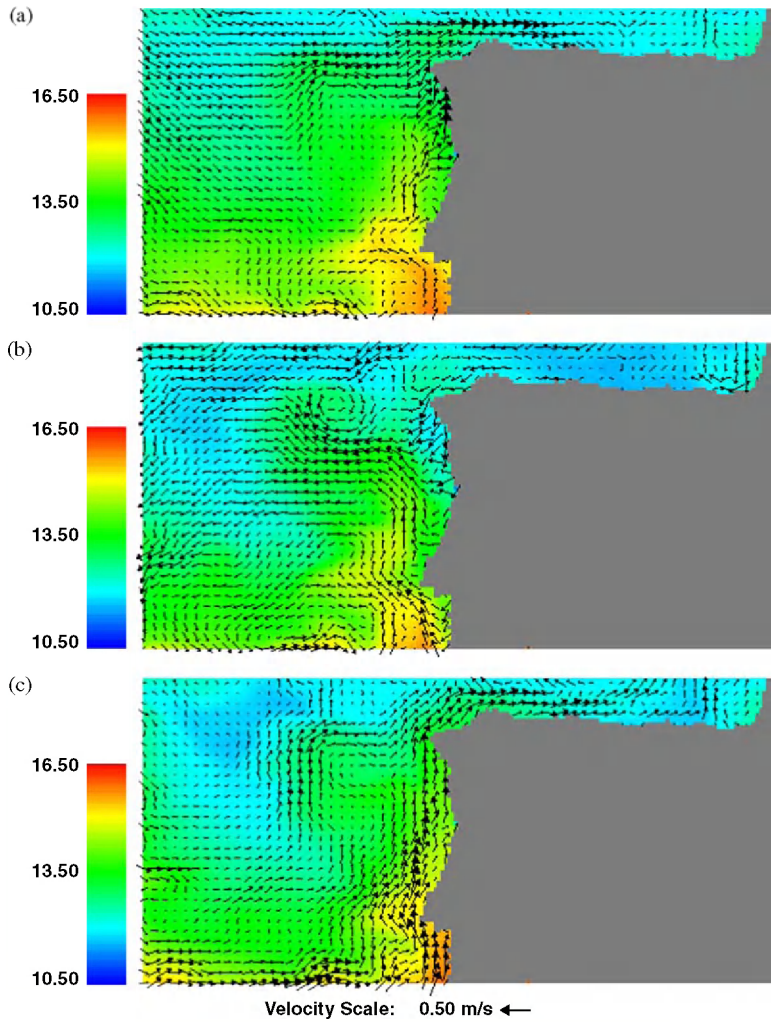

Figure 3. (a) Horizontal velocity after 31 days of real wind; (b) horizontal velocity after 44 days of real wind; (c) horizontal velocity after 44 days of northerly wind. The colour scale bar indicates temperature (°C).

constant wind simulation only a few tracers left the coastal region (around 5% at day 45), whereas in the real wind simulation more than 50% were exported offshore at the end of the larval period. Figure 4b shows the percentage of tracers that remained in the region where larval food is more abundant, i.e. the coastal area till the 1000-m isobath and above 100-m depth (or 200 m depending on the larval prey layer thickness). As expected, the highest final values (between 65% and 90%) occurred in the northerly constant wind simulations although, during the first 20 days, real wind simulations result in larger values of larval retention than the northerly constant wind simulation with a larval prey layer thickness of 100 m. This can be explained by the downwelling movement associated with a northerly wind that pushes tracers below 100-m depth. Figure 4c highlights the relation between the meridional component of the windstress (Figure 1a) and the percentage of larvae transported offshore in the real wind case (Figure 4a). Some phase lag between the two curves was expected because of inertia. Initially the system reacts to the short bouts of wind upwelling events, as can be seen by the changing slope of the offshore transport curve during the first 15 days. Then the slope stabilizes and, somewhere between days 23 and 33, the offshore transport of larvae decreases because the northern component of the wind-stress intensifies. Shortly after (around day 37), the curve of the offshore transport shows its maximum slope in agreement with the intensification of the southerly winds. The offshore transport affects the larval biomass, as can be seen in Figure 5. The simulations with a 200-m larval prey layer thickness (Figure 5a, curves 3 and 4) yielded higher biomass results than the simulations done with a 100-m layer (Figure 5a, curves 1 and 2). Comparing the northerly constant wind with the real wind simulation, for a 200-m

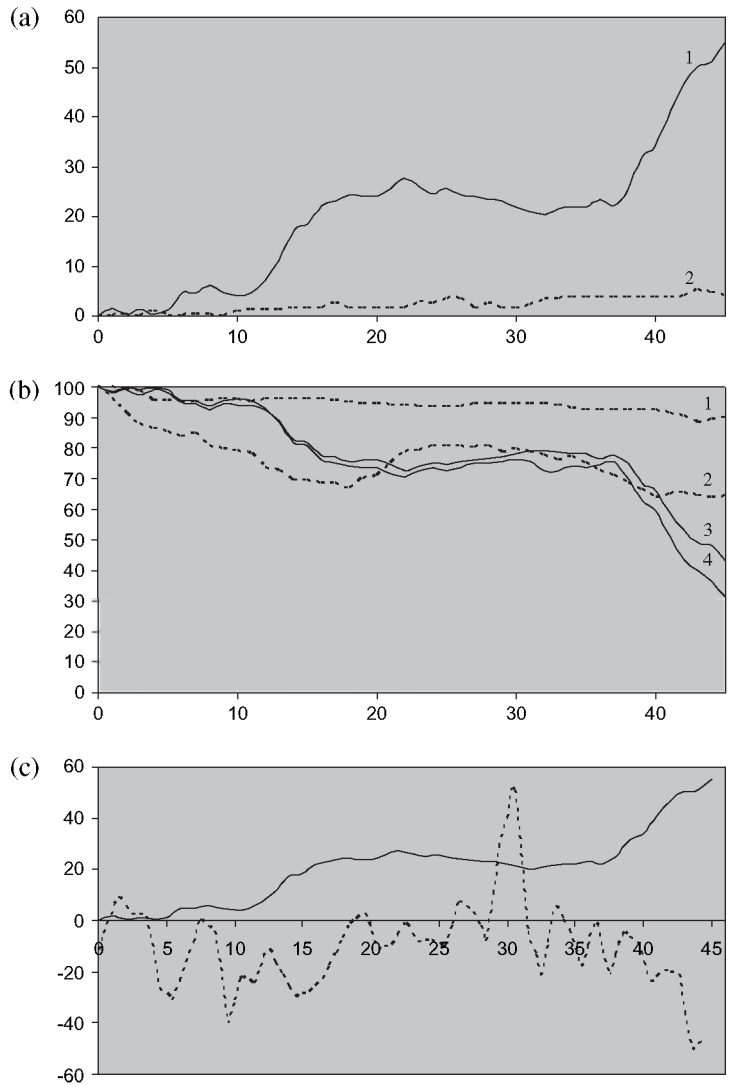

Figure 4. (a) Percentage of larvae that cross the 1000-m isobath. Curve 1: real wind; Curve 2: northerly constant wind. (b) Percentage of larvae that did not cross the 1000-m isobath and remained above 100-m depth (or 200-m depth). Curve 1: northerly constant wind with a larval prey layer thickness of 200 m; Curve 2: northerly constant wind with a larval prey layer thickness of 100 m; Curve 3: real wind with a larval prey layer thickness of 200 m; Curve 4: real wind with a larval prey layer thickness of 100 m. (c) Percentage of larvae that cross the 1000-m isobath in the real wind simulation (solid line) and meridional windstress (dotted line – factor scale 50 Pa).

layer, the constant wind simulation coincides with the highest values of biomass (Figure 5a, curve 3 versus curve 4) but for a layer of 100 m the real wind simulation is more favourable (Figure 5a, curve 2 versus curve 1), showing only a slight inversion at the end ($e_{12} = 5.7\%$). This means that when larval prey are less abundant, other factors such as water temperature control larval growth.

Larval prey effect

Curves 3 in Figure 5b (real wind) and c (northerly constant wind) represent the evolution of biomass assuming no restrictions on larval food. They are almost coincident, with slightly higher values in Figure 5c because in the northerly wind simulation there is a downward movement of larvae to regions where temperature is lower. To see the effect of larval prey abundance on growth, curve 3 should be compared with curves 1 and 2. The first conclusion is that without food restrictions, larval biomass reaches the maximum value. This is especially evident in the real wind case where curve 3 appears detached from the others, which means that variations in the availability of larval prey have a greater impact on biomass production in the real wind case. By comparing Figure 5b and c one could also say that

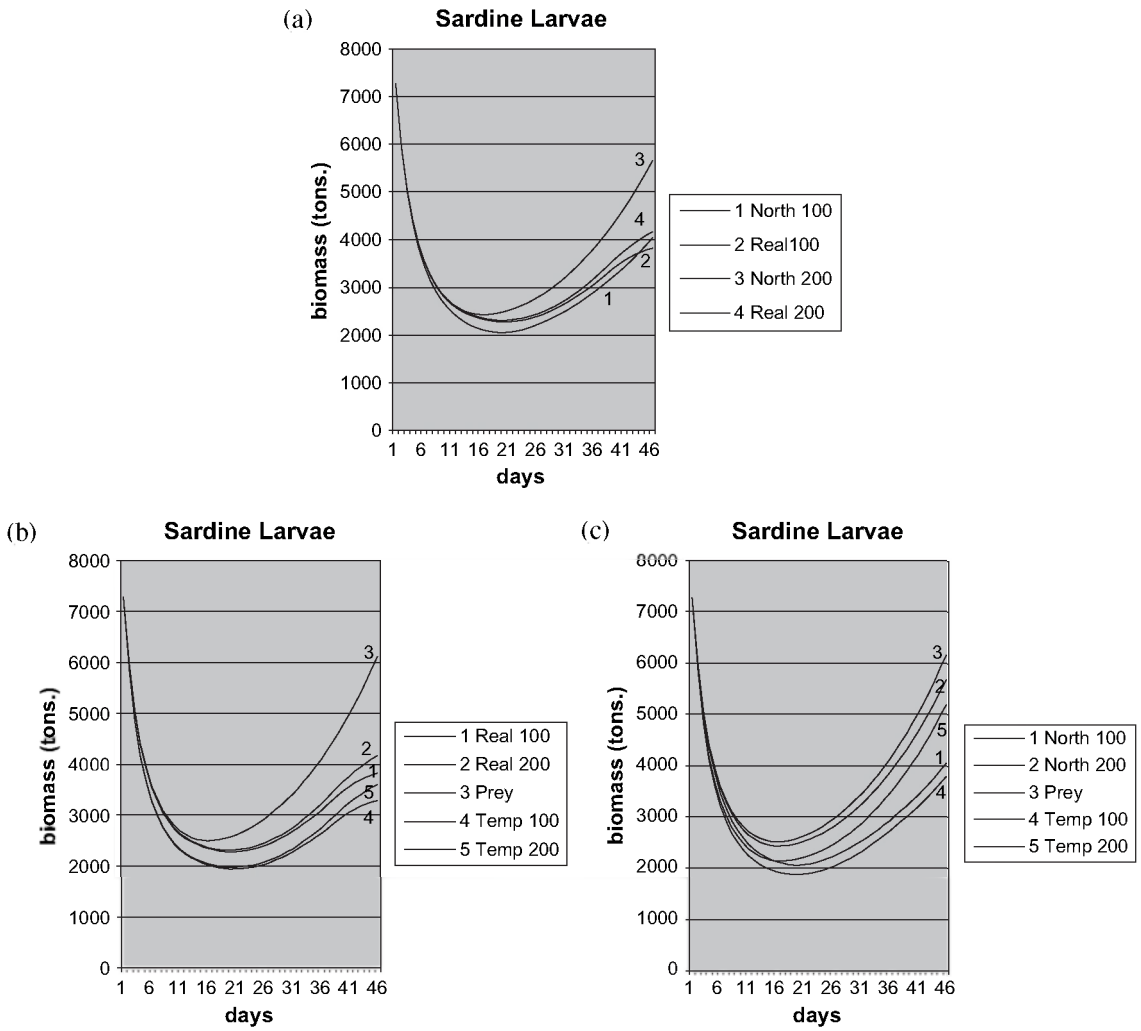

Figure 5. (a) Biomass changes for northerly and real wind with larvae layer thicknesses of 100 m and 200 m; (b) biomass changes for real wind with larvae layer thicknesses of 100 m and 200 m. Curves 1 and 2 include temperature and nutrient corrections, curve 3 temperature correction only and curves 4 and 5 nutrient correction only; (c) same as (b) for northerly wind.

the main difference between real and constant northerly wind simulations is the increase of biomass in curves 2 and 5 of Figure 5c. Changing larval prey layer thickness from 100 m to 200 m has a greater impact on the northerly constant wind simulation. This result was expected since larvae are initially spread from the sea surface to a depth of 100 m and, during a downwelling regime, some of them sink, moving away from the region where larval prey are present, especially when the larval prey layer thickness is equal to 100 m.

Temperature effect

Curves 4 and 5 in Figure 5b and c represent the biomass evolution without the temperature effect for the real and northerly wind cases. To see how temperature affects the results they should be compared with curves 1 and 2. Table 2 shows that $e_{41} = -14.2\%$, $e_{52} = -13.6\%$ for the real wind simulation, and $e_{41} = -6.4\%$, $e_{52} = -8.4\%$ for the northerly constant wind, which means that the temperature effect in the former case is more important because larvae are surrounded by cold water when an upwelling event occurs (real wind simulation), which favours the increase in biomass (considering Houde and Zastrow's equations, the net effect of a temperature decrease on growth and mortality favours growth).

Comparing the larval prey and temperature effects one could say, looking at Figure 5b and c or Table 2, that the effect of larval prey is of greater significance to larval production except in one case, where both have the same

order of magnitude (Figure 5b and c) ($e_{52} = -8.4\%$, $e_{32} = 8.6\%$), which means that, for the northerly constant wind simulation and for a larval prey layer thickness of 200 m, the increase in larval biomass with no food restrictions is similar to the increase in larval biomass when the temperature effect is considered.

Discussion

In this paper we analysed the effects of temperature and food availability on larval survival for two extreme scenarios of windforcing. Comparing the real and northerly wind simulations for a depth of larval prey equal to 100 m we can say that, as long as larvae remain in the region of the continental shelf, they have better survival conditions in the former simulation, because in the latter they move down to a region where food is absent. Near the end of the larval period, when many larvae were transported offshore (around 50% in the real wind simulation), larval biomass in the northerly wind simulation recovers (curve 1 in Figure 5a) and the temperature effect (cold water in the bottom) is enhanced. For the 200 m case the biomass in the northerly wind simulation is always larger because, in spite of the downward movement, larvae never reach an oligotrophic region. This study also shows that short bouts of upwelling can have significant impacts on the distribution of larvae (Figures 2b and 4c) and explain why the effects of spatial variations in food availability (curve 3 in Figure 5b and c) have a greater impact on the overall change in biomass of larval cohorts than the effect of temperature (curves 4 and 5 in Figure 5b and c). Several papers suggest a link between the interannual variability in windforcing and the interannual variability in fish survival and recruitment. Hannah *et al.* (2000) pointed out the importance of the circulation variability for haddock larval survival in the Browns Bank region. The circulation changes associated with the variable windforcing can amplify the roles of drift and retention. Potential consequences include differences in food availability, temperature, exposure to predators, and probability of recruitment to resident populations. Mountain *et al.* (2003) suggested that the interannual variability in egg mortality rate for cod and haddock during the US GLOBEC Georges Bank program (1995–1999) was associated with the interannual variability in windforcing. Two extreme cases were compared that show some resemblance with the two wind scenarios of our analysis. In 1997 the wind-driven movement of eggs was largely across the isobaths and nearly all the eggs were lost. In contrast, in 1998 the wind-driven movement was mainly parallel to isobaths and most eggs remained on the bank and survived. In our study, comparing the northerly constant wind simulation (wind driven movement parallel to isobaths) with the real wind case (wind driven movement mainly across the isobaths) for a larval prey layer thickness of 200 m, the final value of larval biomass in the former case was 36% higher (curves 3 and 4 of Figure 5a).

The model used in our simulations does not account for two important factors: river plumes and primary production. These factors may increase the total larval biomass for the real wind simulation. River plumes affect larval retention and may contribute to their survival. The distribution and offshore transport of sardine eggs and larvae on the Iberian coast is not just determined by wind action. The Western Iberia Buoyant Plume (WIBP), the Iberian Poleward Current (IPC) and its associated mesoscale structures, as well as the interaction between the poleward flow and the buoyant plume (Santos *et al.*, 2004) also contribute to drift and retention mechanisms. The WIBP is low-salinity surface water fed by the winter-intensified run-off of several rivers (Minho, Mondego, Douro, Lima, Vouga) on the northwest coast of Portugal and Spain. During typical non-upwelling winter conditions the plume is confined to the inner shelf, from the Mondego river mouth northward. As the plume expands offshore during an upwelling event, it provides a vertical retention mechanism of the larvae close to the shelf break. According to Govoni and Chester (1990), Grimes and Finucane (1991), and Sabatés *et al.* (2001), the plumes of continental freshwater are habitats that afford conditions favourable to the growth and survival of fish larvae. Aside from this mechanism of vertical retention, there is a mechanism for horizontal retention that results from the fact that the poleward slope-flow (the IPC) acts as a barrier to offshore Ekman transport, retaining most of the plume close to the slope. In years of strong poleward flow and an enlarged plume, the negative impact of coastal upwelling on transport is reduced. The second factor concerns primary production. The "Optimal Environmental Window" (OEW) hypothesis of Cury and Roy (1989) suggests that the spawning season is not related to the seasonal occurrence of upwelling, but rather to the seasonal occurrence of windspeed of $5-6\ m\ s^{-1}$ (Roy *et al.*, 1992). In areas where windspeed during the upwelling season is close to, or lower than the threshold value of $6\ m\ s^{-1}$, small-scale turbulence increases the encounter rate between larvae and prey, and spawning takes place during the upwelling season in order to benefit from enhanced primary production and food availability. In areas where windspeed during the upwelling season is higher than the threshold value, spawning occurs outside the upwelling season because high windspeed generates strong turbulence that desegregates food and larvae patches (Peterman and Bradford, 1987), promotes larval offshore transport, and creates a strong mixed layer and a light-limited phytoplankton population, therefore reducing primary production and zooplankton biomass (Huntsman and Barber, 1977). Considering that the windstress magnitude is equal to $\tau = \rho_a C_D W^2$ (Pond and Pickard, 1983) where $\rho_a = 1.3\ kg\ m^{-3}$ is the density of air, $C_D = 1.4 \times 10^{-3}$ the drag coefficient, and W the windspeed in $m\ s^{-1}$,

a windspeed equal to $6\,m\,s^{-1}$ gives a critical windstress $\tau = 0.066$ Pa. Figure 1a shows that the meridional component of the windstress is higher than this critical value. According to the OEW hypothesis, this means that offshore transport and wind mixing are the limiting factors that control recruitment variability. However, the retention mechanism described above concerning the interaction between river plumes and the poleward slope-flow (the IPC), acts as a barrier to offshore Ekman transport. This retention mechanism associated with the increase in primary production during an upwelling event may favour larval survival.

Aside from fronts, other structures, such as filaments and gyres, affect larval transport and retention (Rodriguez *et al.*, 1999; Hannah *et al.*, 2000; Brickman *et al.*, 2001). The simulation of these features imposes some numerical problems related to the horizontal resolution of the forcing functions and the circulation model itself. The windstress fields and the monthly climatological density fields used in the simulations have a resolution of 1°, which is interpolated onto the model grid. This means that small-scale fronts, mesoscale vortices, and filaments are not resolved by the model. The coarse resolution of the input data and of the circulation model may not be ideal for studies of mesoscale phenomena (Bartsch and Coombs, 1997). The resolution of the circulation model is also inappropriate to simulate fine details of the biological model such as the prey encounter and capture processes and the relationship between these and growth (Heath and Gallego, 1998).

In future work, instead of imposing larval prey layer thickness, as we did, the numerical model should be able to compute it. This would require a definition of sardine larvae prey and the parameterization of the biological and physical processes involved in the food chain, such as the vertical transport of nutrients related to an upwelling event which can enhance biological activity and total larval biomass, for certain values of windspeed. Behavioural characteristics such as vertical migration should be included as they may influence horizontal dispersion (Bartsch *et al.*, 1989). Bio-physical modelling should also consider the run-off of several rivers on the northwest coast of Portugal because they contribute to retention mechanisms that affect larval survival.

Acknowledgements

This work was carried out with the financial support of the Portuguese Science Foundation (FCT), as part of the project "Assessing the Impact of Hydrodynamical Forcing on the Survival of Small Pelagic Fish Early Stages of Western Iberia" (SURVIVAL). SURVIVAL is affiliated with IGBP core project GLOBEC and the PELAGICOS programme (IPIMAR-FCT POCTI/PLE/13/00). We thank Pierre Pepin, consultant for this project, and Pedro Ré for their relevant remarks and Amanda Booth for help in the revision of this article.

References

Adcroft, A., Hill, C., and Marshall, J. 1997. Representation of topography by shaved cells in a height coordinate ocean model. Monthly Weather Review, 125: 2293–2315.

Alemany, F., and Álvarez, F. 1994. Formation of initial daily increments in sagittal otoliths of reared and wild *Sardina pilchardus* yolk-sac larvae. Fishery Bulletin US, 95: 187–194.

Arhan, M., Colin de Verdiére, A., and Mémery, L. 1994. The eastern boundary of the subtropical Atlantic. Journal of Physical Oceanography, 24: 1295–1316.

Backhaus, J. O. 1985. A three-dimensional model for the simulation of shelf sea dynamics. Deutsche Hydrographische Zeitschrift, 38: 165–187.

Bakun, A. 1996. Patterns in the Ocean. Ocean Processes and Marine Population Dynamics. University of California Sea Grant/Centro de Investigaciones Biológicas de Noroeste, San Diego, CA, USA/La Paz, Baja California Sur, Mexico. 323 pp.

Bartsch, J., Brander, K., Heath, M., Munk, P., Richardson, K., and Svendsen, E. 1989. Modelling the advection of herring larvae in the North Sea. Nature, 340: 632–636.

Bartsch, J., and Coombs, S. 1997. A numerical model of the dispersal of blue whiting larvae, *Micromesistius poutassou* (Risso), in the eastern North Atlantic. Fisheries Oceanography, 6: 141–154.

Batteen, M. L., Martinez, J. R., Bryan, D. W., and Buch, E. J. 2000. A modeling study of the coastal eastern boundary current system off Iberia and Morocco. Journal of Geophysical Research, 105: 14173–14195.

Borges, M. F., Santos, A. M. P., Crato, N., Mendes, H., and Mota, B. 2003. Sardine regime shifts off Portugal: a time series analysis of catches and wind conditions. Scientia Marina, 67: 235–244.

Brickman, D., Schakell, N. L., and Frank, K. T. 2001. Modelling the retention and survival of Browns Bank haddock larvae using an early life stage model. Fisheries Oceanography, 10: 284–296.

Burchard, H., Bolding, K., and Villarreal, M. R. 1999. GOTM, A General Ocean Turbulence Model. Theory, implementation and test cases. European commission, Report EUR 18745 EN, 103 pp.

Cowan, J. Jr., Rose, K., Houde, E., Wang, S., and Young, J. 1999. Modeling effects of increased larval mortality on bay anchovy population dynamics in the mesohaline Chesapeake Bay: evidence for compensatory reserve. Marine Ecology Progress Series, 185: 133–146.

Cury, P., and Roy, C. 1989. Optimal environmental window and pelagic fish recruitment success in upwelling areas. Canadian Journal of Fisheries and Aquatic Sciences, 46: 670–680.

Dickson, R. R., Kelly, P. M., Colebrook, K. M., Wooster, W. S., and Cushing, D. H. 1988. North winds and production in the eastern North Atlantic. Journal of Plankton Research, 10: 151–169.

Ferreira, A. 1970. O Clima de Portugal. Normais Climatológicas do Continente, Açores e Madeira correspondentes a 1931–1960, 2nd edn. Serviço Meteorológico Nacional, Lisboa.

Flather, R. A. 1976. A tidal model of the northwest European continental shelf. Memoires de la Society Royal des Sciences de Liege, 6: 141–164.

Gaspar, P. G., Grégoris, Y., and Lefevre, J. M. 1990. A simple eddy kinetic energy model for simulations of the oceanic vertical mixing: tests at station Papa and Long-term Upper Ocean Study site. Journal of Geophysical Research, 95: 16179–16193.

Govoni, J. J., and Chester, A. J. 1990. Diet composition of larval *Leiostomos xanthurus* in and about the Mississippi River. Journal of Plankton Research, 12: 819–830.

Grimes, C. B., and Finucane, J. H. 1991. Spatial distribution and abundance of larval and juvenile fish, chlorophyll and macrozooplankton around the Mississippi River discharge plume and the role of the plume in fish recruitment. Marine Ecology Progress Series, 75: 109–119.

Hannah, C. G., Shore, J. A., and Loder, J. W. 2000. The drift-retention dichotomy on Browns Bank: a model study of interannual variability. Canadian Journal of Fisheries and Aquatic Sciences, 57: 2506–2518.

Heath, M. R., and Gallego, A. 1997. From the biology of the individual to the dynamics of the population: bridging the gap in the fish early life studies. Journal of Fish Biology, 51(Suppl. A): 1–29.

Heath, M. R., and Gallego, A. 1998. Bio-physical modelling of the early life stages of haddock, *Melanogrammus aeglefinus*, in the North Sea. Fisheries Oceanography, 7: 110–125.

Houde, E. D. 1989. Comparative growth, mortality, and energetics of marine fish larvae: temperature and implied latitudinal effects. Fishery Bulletin US, 87: 471–495.

Houde, E. D. 1996. Evaluating stage-specific survival during the early life of fish. *In* Survival Strategies in Early Life Stages of Marine Resources, pp. 51–66. Ed. by Y. Watanabe, Y. Yamashita, and Y. Oozeki. Balkema, Rotterdam. 367 pp.

Houde, E. D. 1997. Patterns and trends in larvae-stage growth and mortality of teleost fish. Journal of Fish Biology, 51(Suppl. A): 52–83.

Houde, E. D., and Zastrow, C. E. 1993. Ecosystem and taxon specific dynamic and energetics properties of larval fish assemblages. Bulletin of Marine Science, 53: 290–335.

Huntsman, S. A., and Barber, R. T. 1977. Primary production off northwest Africa: the relationship to wind and nutrients conditions. Deep-Sea Research, 24: 25–33.

Leendertsse, J., and Liu, S. 1978. A three-dimensional turbulent energy model for non-homogeneous estuaries and coastal sea systems. *In* Hydrodynamics of Estuaries and Fjords, pp. 387–405. Ed. by J. C. J. Nihoul. Elsevier, Amsterdam.

Lett, P. F., and Kohler, A. C. 1976. Recruitment: a problem of multispecies interaction and environmental perturbations, with special references to Gulf of St. Lawrence Atlantic herring (*Clupea harengus harengus*). Journal of the Fisheries Research Board of Canada, 33: 1353–1371.

Levitus, S., Burgett, R., and Boyer, T. P. 1994. World Ocean Atlas 1994. NOAA Atlas NESDIS 3, vols. 1 and 2. 99 pp.

Lo, N. C. H., Smith, P. E., and Butler, J. L. 1995. Population growth of northern anchovy and Pacific sardine using stage-specific matrix models. Marine Ecology Progress Series, 127: 15–26.

Martins, F. A., Neves, R. J., and Leitão, P. C. 1998. A three-dimensional hydrodynamic model with generic vertical coordinate. *In* Proceedings of Hydroinformatics'98, vol. 2, pp. 1403–1410. Ed. by V. Babovic, and L. C. Larsen. Balkema, Rotterdam.

Martins, F. A., Leitão, P. C., Silva, A., and Neves, R. J. 2000. 3D modelling in the Sado estuary using a new generic vertical discretization approach. Oceanologica Acta, 24: 51–62.

Mohn, R. 1991. Stability and sustainability of harvesting strategies in a modelled fishery. *In* Management under Uncertainties Related to Biology and Assessments, with Case Studies on Some North Atlantic Fisheries. Northwest Atlantic Fisheries Organ 16. Dartmouth (NS), Canada. pp. 133–135.

Moita, M. 2001. Estrutura, Variabilidade e Dinâmica do Fitoplâncton na Costa de Portugal Continental (in Portuguese). PhD dissertation, FCUL, Lisbon: 272 pp.

Mountain, D. G., Green, J., Sibunka, J., and Johnson, D. 2003. The transport of cod, *Gadus morhua*, and haddock, *Melanogrammus aeglefinus*, on Georges Bank 1995–1999. ICES CM 2003/O:5. 24 pp.

Myers, R. A. 1991. Recruitment variability and range of three fish species. *In* Management under Uncertainties Related to Biology and Assessments, with Case Studies on Some North Atlantic Fisheries. Northwest Atlantic Fisheries Organ 16. Dartmouth (NS), Canada. pp. 21–24.

Oey, L., and Chen, P. 1992. A model simulation of circulation in the northeast Atlantic shelves and seas. Journal of Geophysical Research, 97: 20087–20115.

Palma, E. D., and Matano, R. P. 2000. On the implementation of passive open boundary conditions for a general circulation model: the three-dimensional case. Journal of Geophysical Research, 105: 8605–8627.

Paillet, J., and Mercier, H. 1997. An inverse model of the eastern North Atlantic general circulation and thermocline ventilation. Deep-Sea Research, 44: 1293–1328.

Pepin, P. 1991. Effect of temperature and size on development, mortality, and survival rates of the pelagic early life history stages of marine fish. Canadian Journal of Fisheries and Aquatic Sciences, 48: 503–518.

Peterman, M. R., and Bradford, M. J. 1987. Wind speed and mortality rate of a marine fish, the northern anchory (*Engraulis Mordax*). Science, 235: 354–356.

Pond, S., and Pickard, G. L. 1983. Introductory Dynamical Oceanography. Pergamon, New York. 329 pp.

Ré, P. 1986. Ecologia da postura e da fase planctónica da *Sardina pilchardus* (Walbaum 1792) na região central da costa Portuguesa. Boletim da Sociedade Portuguesa de Ciências Naturais (in Portuguese), 23: 5–81.

Ribeiro, R. 1991. Ecologia do Ictioplâncton e Reprodução da Anchova (in Portuguese). PhD dissertation, FCTUC, Coimbra: 356 pp.

Roy, C., Cury, P., and Kifany, S. 1992. Pelagic fish recruitment success and reproductive strategy in upwelling areas: environmental compromises. *In* Benguela Trophic Functioning. Ed. by A. I. L. Payne, K. H. Mann and R. Hilborn, South African Journal of Marine Science, 12: 135–146.

Rodriguez, J. M., Heŕndez-León, S., and Barton, E. D. 1999. Mesoscale distribution of fish larvae in relation to an upwelling filament off Northwest Africa. Deep-Sea Research, 46: 1969–1984.

Sabatés, A., Salat, J., and Olivar, M. P. 2001. Advection of continental water as an export mechanism for anchovy, *Engraulis encrasicolus*, larvae. Scientia Marina, 65: 77–87.

Santos, A. 1995. Modelo hidrodinâmico de circulação oceânica e estuarina (in portuguese). PhD dissertation, IST, Lisbon: 273 pp.

Santos, A. M. P., Borges, M. F., and Groom, S. 2001. Sardine and horse mackerel recruitment and upwelling off Portugal. ICES Journal of Marine Science, 58: 589–596.

Santos, A. M. P., Peliz, A., Dubert, J., Oliveira, P. B., Angélico, M. M., and Ré, P. 2004. Impact of a winter upwelling event on the distribution and transport of sardine (*Sardina pilchardus*) eggs and larvae off western Iberia: a retention mechanism. Continental Shelf Research, 24: 149–165.

Trenberth, K. E., Large, W. G., and Olsen, J. G. 1990. The mean annual cycle in global wind stress. Journal of Physical Oceanography, 20: 1742–1760.